JOURNAL OF GEOPHYSICAL RESEARCH, VOL. 104, NO. B12, PAGES 28,899–28,914, DECEMBER 10, 1999

Friction of simulated fault gouge for a wide range of velocities and normal stresses

Karen Mair and Chris Marone

Department of Earth, Atmospheric and Planetary Sciences, Massachusetts Institute of Technology, Cambridge

Abstract. During earthquake rupture, faults slip at velocities of cm/s to m/s. Fault friction at these velocities strongly influences dynamic rupture but is at present poorly constrained. We study friction of simulated fault gouge as a function of normal stress (σ_n = 25 to 70 MPa) and load point velocity (V= 0.001 to 10 mm/s). Layers of granular quartz (3 mm thick) are sheared between rough surfaces in a direct shear apparatus at ambient conditions. For a constant σ_n, we impose regular step changes in V throughout 20 mm net slip and monitor the frictional response. A striking observation at high velocity is a dramatic reduction in the instantaneous change in frictional strength for a step change in velocity (friction direct effect) with accumulated slip. Gouge layers dilate for a step increase in velocity, and the amount of dilation decreases with slip and is systematically greater at higher velocity. The steady state friction velocity dependence (a-b) evolves from strengthening to weakening with slip but is not significantly influenced by V or σ_n. Measurements of dilation imply that an additional mechanism, such as grain rolling, operates at high velocity and that the active shear zone narrows with slip. Data from slow (μm/s) and fast (mm/s) tests indicate a similar displacement dependent textural evolution and comparable comminution rates. Our experiments produce a distinct shear localization fabric and velocity weakening behavior despite limited net displacements and negligible shear heating. Under these conditions we find no evidence for the strong velocity weakening or low friction values predicted by some theoretical models of dynamic rupture. Thus certain mechanisms for strong frictional weakening, such as grain rolling, can likely be ruled out for the conditions of our study.

1. Introduction

During earthquake rupture, geological faults slip at a wide range of velocities (up to m/s) and generate significant amounts of gouge. Friction at these conditions is important in determining the characteristics of seismic rupture, for example, rupture mode, stress drop, fault healing rate, shear heating, and fault zone development. Although many detailed studies of rock friction have been carried out in the laboratory at low slip velocities, relatively few studies exist to constrain friction constitutive parameters at high velocities. In this paper we present results from systematic experiments on simulated fault gouge spanning a wide range of velocities (0.001-10 mm/s) and normal stresses (25-70 MPa). Our approach is to conduct experiments on a simple system with the aim of identifying the underlying physics associated with certain frictional responses and loading conditions. We aim to isolate the influence of velocity and normal stress by using a standard direct shear geometry and comparable gouge material to that used in previous work at lower velocities. We determine the friction constitutive parameters from velocity stepping tests and measure the velocity and history dependence of friction and dilation. We repeat slow tests to tie in with existing data.

Our aims are to extend the range of parameters available for constraining rate and state friction laws (widely used to model earthquake faulting), to understand the structural development of the gouge, and essentially, to determine how all these aspects compare to the same parameters measured at lower slip velocities.

The frictional response to a change in slip rate is generally described in terms of rate and state constitutive laws [*Dieterich,* 1978, 1979; *Ruina,* 1983]. Recent reviews of the friction laws and their application to seismic faulting are found in the works by *Marone* [1998] and *Scholz* [1998]; therefore only a brief summary is given here. In response to an imposed step increase in loading rate there is a transient increase in friction, termed the direct effect (a), followed by a gradual decrease in friction known as the evolution effect (b). The direct effect is always positive, and is thus an instantaneous viscosity, whereas the evolution effect is generally negative, that is, friction decreases for an increase in velocity. The combination of both effects produces a change in sliding friction called the steady state velocity dependence, or friction rate dependence (a-b). The slip required for friction to evolve to a new steady state is known as the critical slip distance (D_c). Positive velocity dependence, $(a\text{-}b) \geq 0$, corresponds to a velocity strengthening regime, which is inherently stable. Stability controls fault dynamics, and in this regime fault nucleation and propagation are inhibited. In contrast, $(a\text{-}b) < 0$ defines the velocity weakening field that can be either unstable or conditionally stable. Earthquakes can propagate in both cases but can nucleate only in the unstable field. In the context of rate and state friction laws, velocity weakening is a necessary condition for instability [*Rice and Ruina,* 1983].

Friction at high velocities has a major influence on the mode of dynamic rupture. Modeling studies have proposed two different modes of rupture [e.g., *Perrin et al.,* 1995; *Andrews and Ben-Zion,* 1997]: (1) cracklike rupture, consisting of growth of an enlarging, self-similar shear crack; and (2) slip

Copyright 1999 by the American Geophysical Union.

Paper number 1999JB900279.
0148-0227/99/1999JB900279$09.00

pulse rupture [e.g., *Heaton,* 1990], in which only a portion of the eventual rupture area is active at any given instant and risetime is short compared with the total rupture duration. *Heaton*'s [1990] slip pulse model was based on a specific self-healing friction mechanism, but slip pulse rupture can also be generated by other mechanisms, depending on fault prestress, fault heterogeneity, and friction parameters [*Zheng and Rice,* 1994; *Chen and Marone,* 1995; *Perrin et al.,* 1995; *Beeler and Tullis,* 1996; *Zheng,* 1997]. The interactions between constitutive parameters and loading conditions are complex and require numerical modeling; however, factors that seem to favor a rupture pulse mode include (1) low remote stress; (2) high sliding velocity; (3) extreme velocity weakening ($a-b$)<<0 ; (4) $a/b \sim 0.1$ (typical laboratory values are a/b~0.8 for $V = 1$ μm/s); (5) relatively large D_c ; and (6) time dependent aging of frictional strength.

Each rupture model is consistent with some features observed in earthquakes, but it is unclear which (if either) model is correct. Friction studies at high velocity may help determine which rupture mode is more likely. Previous work has shown that friction velocity dependence of granite surfaces varies with slip rate [*Blanpied et al.,* 1987; *Kilgore et al.,* 1993; *Blanpied et al.,* 1998]. In addition, preliminary work on gabbro surfaces indicates that dynamic friction varies appreciably at high velocity under some conditions [*Tsutsumi and Shimamoto,* 1997].

2. Experimental Technique

Recent studies of rock friction have used two standard approaches to obtain friction constitutive parameters: slide-hold-slide tests where loading is interrupted for a given time; and velocity stepping tests. In this study we concentrate on velocity stepping tests (where decade step changes in load point velocity are applied to a sample under constant normal stress). Our experimental work is designed to explore the influence of velocity and normal stress on friction and shear heating [K. Mair and C. Marone, Shear heating in granular layers, submitted to *Pure and Applied Geophysics*, 1999, hereinafter Mair and Marone, submitted manuscript, 1999]; therefore we carry out two series of tests to study (1) velocity (0.001-10 mm/s) for constant normal stress (25 MPa) and (2) normal stress (25-70 MPa) for uniform velocity (stepped between 0.3-3 mm/s). The tests were all performed at room temperature and humidity.

Figure 1 presents the sample geometry. Layers of simulated quartz gouge (3 mm thick) are sheared between grooved steel forcing blocks in a servo controlled double direct shear apparatus. Grooved steel surfaces approximate conditions of rough rock surfaces, and by inhibiting boundary slip, force shear to occur within the layers [*Marone et al.,* 1990]. The gouge consists of Ottawa sand (a pure, >99.7 %, quartz sand obtained from the US Silica Company, Ottawa, Illinois) and has an initial grain size range of 50-150 μm. The biaxial loading apparatus applies horizontal forces to the side blocks and a vertical motion to the middle block. The steel forcing blocks have a surface area of 50x50 mm^2. Lubricated Teflon plates fixed to the side blocks minimize gouge loss from unconfined lateral edges of the sample. Lubricated copper shims on the base of the sample allow the side blocks to move horizontally in response to shear displacement and help prevent gouge loss from the base of the sample. A thermocouple located in one steel side block measures temperature near the fault zone [Mair and Marone, submitted manuscript, 1999].

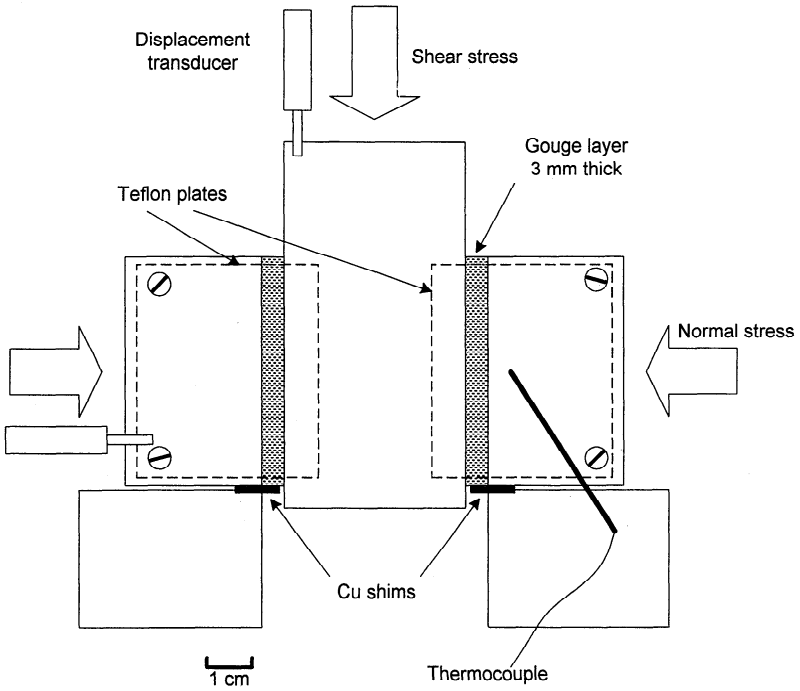

Figure 1. Schematic diagram of the sample geometry showing 3-mm-thick quartz gouge layers between a three-block steel sample. The orientation of shear and normal applied stresses are indicated, as are the locations of displacement transducers, the thermocouple, and two steel support blocks. Lubricated copper shims are attached to the underside of the side blocks, and four lubricated Teflon plates are attached to the unconfined faces (front and back) of the sample (two shown as dotted lines).

Shear and normal displacements are measured with 0.1 μm resolution throughout the tests by displacement transducers located on the vertical and horizontal rams, respectively (Figure 1). Load cells on both rams monitor shear and normal load continuously throughout the tests, with 0.1 kN resolution. We record data at up to 3000 samples/s (depending on the velocity of the experiment), which gives a spacing of 3.5 μm between data points at the highest velocity (V = 10 mm/s) and significantly higher resolution at slower V. This resolution is adequate to capture the characteristics of the friction response (see the appendix for details). We assume that a constant gouge surface area of 2500 mm^2 is maintained throughout the test and, therefore, that normal load can be converted into normal stress by simple division by the surface area. From examination of the gouge layers after an experiment, this is a reasonable assumption provided Teflon plates are attached to the side blocks. Further discussion of the influence of Teflon plates is discussed in the appendix.

Our test procedure involves application of the appropriate normal stress, after which load is applied to the center steel block through a sequence of constant velocity intervals. Normal stress (σ_n) is held constant throughout the test by servo control in load feedback. The displacement required to maintain constant normal stress gives a measurement of the total change in gouge layer thickness and is recorded throughout the test. We assume both layers change by an equal amount and simply halve the total change in normal displacement to obtain changes in gouge layer thickness for a single layer. We ignore Poisson distortion associated with the small changes in shear force upon a velocity perturbation, since we calculate that this would contribute < 1.6 μm to the measured changes in layer thickness. Direct measurements across the layers show that this is a valid assumption [*Karner*, 1999]. Decade step changes in load point velocity (V) are imposed on the middle block at regular intervals throughout 20 mm of slip, and the resulting variations in shear load are monitored. The coefficient of friction is the ratio of shear stress to normal stress $\mu = \tau / \sigma_n$. Friction is known to be influenced by net slip in the direct shear geometry [e.g., *Dieterich*, 1981; *Marone and Kilgore*, 1993; *Richardson and Marone*, 1999], therefore, to allow direct comparison between experiments, all were subjected to exactly the same slip history with velocity steps initiated every 1 mm of slip. In each individual test, normal stress is held constant throughout and, with the exception of dual-velocity tests, velocity is toggled between one pair of velocities. Dual-velocity tests use a novel procedure in which the initial section of the test is run at the slowest (or fastest) pair of velocities; then toward the end of the test, load point velocity is changed to the fastest (or slowest) pair of velocities. Dual-velocity tests are designed to investigate the effect of velocity and slip history on friction parameters and are introduced in the discussion. All the tests carried out, including those repeated under identical conditions to check reproducibility, are documented in Table 1. Details of the experimental method, including the reproducibility of tests, the influence of Teflon side plates, and the "crispness" of imposed velocity steps, are presented in the appendix.

Table 1. Experiments

Experiment	σ_n, MPa	V, mm/s
	Velocity Stepping	
m219	25	0.001-0.01
m185	25	0.01-0.1
m199	25	0.01-0.1
m217	25	0.01-0.1
m218	25	0.01-0.1
m160	25	0.03-0.3
m194	25	0.1-1
m195	25	0.1-1
m196	25	0.1-1
m197	25	0.1-1
m156	25	0.3-3
m157	25	0.6-6
m158	25	0.8-8
m159	25	1-10
m190	25	1-10
m191	25	1-10
m192	25	1-10
m181	30	0.3-3
m147	40	0.3-3
m150	40	0.3-3
m177	50	0.3-3
m178	60	0.3-3
m179	70	0.3-3
m180	70	0.3-3
	Dual Velocity	
m227	25	0.01-0.1 / 1-10
m228	25	0.01-0.1 / 1-10
m229	25	0.001-0.01 / 1-10
m230	25	0.001-0.01 / 1-10

Initial gouge layer thickness 3 mm.
Shear displacement 20 mm.
Here σ_n is normal stress and V is velocity.

3. Results

3.1. Friction Data

The frictional response to imposed step changes in velocity (1-10-1 mm/s) is shown in Figure 2a. The velocity history (shown as inverse velocity for ease of comparison with friction data) is given in Figure 2b. The step changes in velocity, indicated by vertical dashed lines, are sharp transitions. Friction shows an abrupt increase and a subsequent exponential decay to a new steady state for a step increase in velocity and the converse for a step decrease [*Dieterich*, 1978, 1979]. At an imposed velocity step we measure $\Delta\mu_{direct}$ as the direct friction effect and $\Delta\mu_{evol}$ as the evolution effect. $\Delta\mu_{ss}$ is the measured change in steady state friction. The parameters $\Delta\mu_{direct}$ and $\Delta\mu_{evol}$ are closely related to the friction parameters a and b, respectively, and indicate the main trends in those parameters. However, modeling is required to obtain the exact values of the constitutive parameters due to elastic interaction of the sample and apparatus. We choose to report measured values rather than model parameters as it is a simpler, more robust technique for documenting the effects of velocity. Also we are more interested in changes in constitutive parameters than in absolute values, so in this paper we concentrate our efforts on reproducibility of the data at new conditions rather than detailed modeling of every case. We carried out limited modeling, presented in Table 2, to establish the range of constitutive parameter values. The friction rate parameter (a-b) can be obtained directly from our measurements.

The coefficient of friction is plotted as a function of shear displacement for a typical high-velocity test in Figure 3a. Throughout this experiment, velocity was stepped between 1 and 10 mm/s at regular slip intervals, and normal stress was

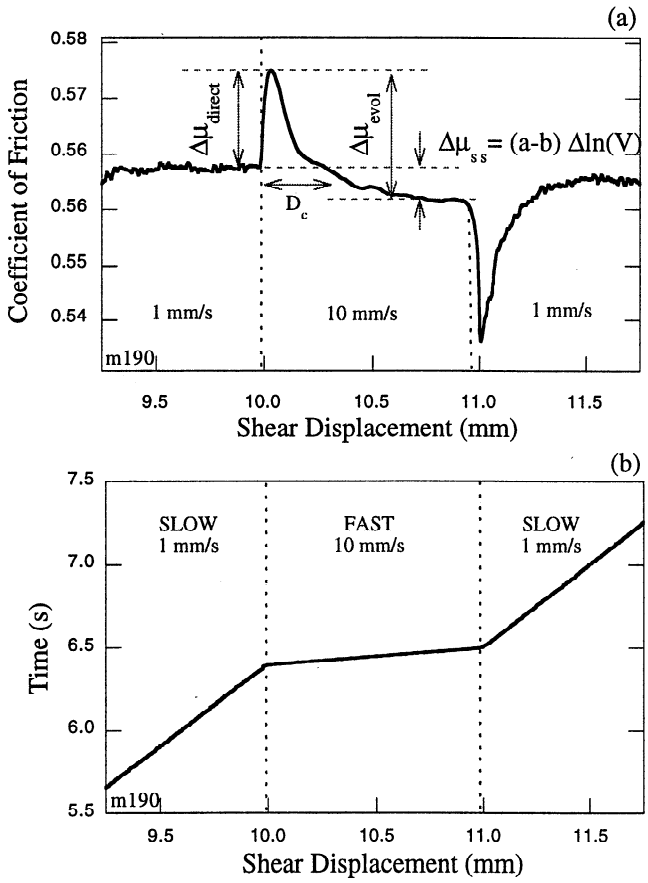

Figure 2. Frictional response to imposed changes in load point velocity from 1 mm/s to 10 mm/s to 1 mm/s. (a) Friction coefficient (shear stress/normal stress) is plotted as a function of shear displacement. Important friction parameters $\Delta\mu_{direct}$, $\Delta\mu_{evol}$, $\Delta\mu_{ss}$, and D_c are introduced. (b) Velocity step is plotted as time versus shear displacement for comparison with Figure 2a; hence the slope indicates inverse velocity.

constant at σ_n = 25 MPa. Friction increases on initial loading, with some macroscopic strain hardening, and then reaches approximately steady state (neutral behavior) after a few millimeters of slip. Second-order direct ($\Delta\mu_{direct}$) and evolution ($\Delta\mu_{evol}$) effects associated with the velocity steps are clearly observed. For the highest velocities a significant reduction in the direct friction effect ($\Delta\mu_{direct}$) is observed with increased displacement (Figure 3). Also shown is the gouge layer thickness of a single layer as a function of slip (Figure 3a). The overall reduction in thickness is due to geometric thinning and compaction [*Scott et al.*, 1994]. Superimposed onto this trend are dilation and compaction events associated with velocity changes. Alpha (α), shown schematically, is the relative change in layer thickness at a velocity step and is discussed in detail below. Figure 3b shows friction as a function of shear displacement for tests carried out at different velocities (steps are factor of 10 changes in all cases) but constant σ_n = 25 MPa to illustrate the influence of velocity. Individual curves are shifted by 0.04 in the y axis for ease of comparison. We observe only minor changes in steady state sliding friction, which ranges between 0.56 and 0.6 for all tests. We assume that trends in this base level of sliding friction do not systematically affect friction parameters and remove these trends before modeling or measuring parameters (following previous workers, e.g., *Marone and Cox* [1994] and *Blanpied et al.* [1998]). Sliding friction exhibits velocity strengthening initially, with a transition to velocity weakening with accumulated net slip (Figure 3b). The magnitude of the direct effect ($\Delta\mu_{direct}$) is independent of slip in the slowest tests, but faster tests show a notable decrease in $\Delta\mu_{direct}$ with increasing displacement. Also, for a given shear displacement the critical slip displacement D_c (i.e., amount of slip required to reach a new steady state) increases systematically with increasing velocity (Figure 4, Table 2). It is interesting to note that this would imply a characteristic time for reequilibration, rather than a characteristic displacement.

Figure 5a shows the coefficient of friction and gouge layer thickness as a function of slip for σ_n = 70 MPa and velocities of 0.3-3 mm/s. Behavior is broadly similar to lower normal stress tests (e.g., Figure 3a). Key differences are a shorter phase of strain hardening followed by an overall weakening in friction, and a more dramatic decrease in $\Delta\mu_{direct}$ with slip. Gouge layer thickness shows overall geometric thinning, plus superimposed compaction and dilation events similar to the equivalent test at lower normal stress (Figure 3a). Figure 5b shows friction as a function of shear displacement for a range of σ_n = 25-70 MPa. Curves are offset in the y axis for clarity (all have friction values close to 0.6). The overall weakening in the latter part of the test, highlighted by dashed lines, is systematically larger as a function of normal stress. The decrease in $\Delta\mu_{direct}$ occurs systematically earlier (i.e., at lower slip), and $\Delta\mu_{direct}$ decrease is larger with increased normal stress. The following sections focus on specific parameters, and all data are derived from step increases in velocity.

3.2. Steady State Friction Velocity Dependence

Figure 6a shows friction velocity dependence (a-b) as a function of shear displacement for a range of loading rates 0.001-10 mm/s and constant σ_n = 25 MPa. A clear transition from velocity strengthening (a-b > 0) to weakening (a-b < 0) is observed with increased displacement, consistent with previous work [*Dieterich*, 1981; *Kilgore et al.*, 1993; *Beeler et al.*, 1996]. This transition occurs between 5 and 10 mm shear displacement. Different experiments carried out at identical conditions illustrate experiment reproducibility. Previous data [*Marone and Kilgore*, 1993] for quartz gouge layers (of fractal grain size distribution) and velocity stepped between 0.001 and 0.01 mm/s at σ_n = 25 MPa (i.e., the lowest velocity range considered in this study), are superimposed. These data show comparable values to the present study for equivalent experimental conditions.

In order to investigate the systematic behavior of velocity dependence, we plot (a-b) for discrete ranges of shear displacement as a function of upstep velocity (Figure 6b). Lines are visual aids showing the main trends for discrete displacement ranges. A clear positive trend is observed with velocity for small shear displacements; that is, the degree of velocity strengthening increases with velocity (solid line with positive slope). At larger displacements, we note that a-b is independent of velocity (dashed line with zero slope).

The effects of normal stress are shown in Figure 7. Within the scatter in the data, the transition distance (from velocity strengthening to weakening) is independent of normal stress (Figure 7a). Plotting (a-b) for discrete ranges of shear displacement indicates that normal stress has a minor positive influence on initial velocity strengthening and similarly enhances subsequent velocity weakening (Figure 7b).

Table 2. Constitutive Parameters

Experiment	V, mm/s	Slip, mm	$\Delta\mu_{direct}$ x10^{-2}	$\Delta\mu_{evol}$ x10^{-2}	a x10^{-2}	a s.d. x10^{-4}	b x10^{-2}	b s.d. x10^{-4}	D_c, μm
m219	0.001-0.01	2	1.51	1.33	0.66	0.51	0.5	0.50	17.8
m219	0.001-0.01	10	1.42	1.52	0.69	1.26	0.78	1.24	7.4
m219	0.001-0.01	18	1.49	1.95	0.87	1.38	0.69	1.33	3.7
m196	0.1-1	2	1.96	1.75	0.85	0.7	0.53	0.64	59.2
m196	0.1-1	10	1.86	1.93	0.83	1.24	0.75	1.18	52.6
m196	0.1-1	18	0.50	1.01	0.23	0.27	0.24	0.26	109.9
m159	1-10	4	2.15	1.04	0.92	3.43	0.91	3.08	108.1
m159	1-10	10	1.22	1.51	0.39	1.14	0.43	1.20	108.8
m159	1-10	20	0.53	0.87	0.20	0.72	0.44	1.93	183.0

Constitutive friction parameters are best fits obtained from inversions of the Dieterich law [e.g., *Marone*, 1998]. They give the standard deviations (s.d.) marked. Here σ_n = 25 MPa for each experiment.

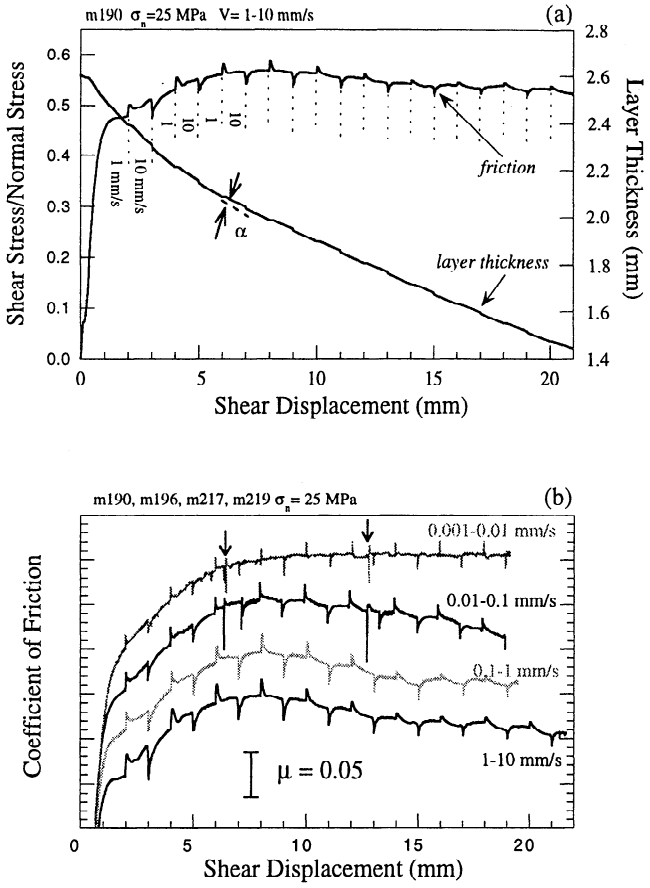

Figure 3. (a) Coefficient of friction and layer thickness as a function of shear displacement for a "fast" velocity test carried out at 1-10 mm/s and σ_n = 25 MPa. The velocity steps are indicated by dashed lines, and alpha is shown schematically. (b) Friction as a function of shear displacement for a range of tests at σ_n = 25 MPa with velocity ranging between 0.001-10 mm/s (all velocity steps are factor of 10 increases and decreases). Curves are offset for clarity since friction levels are comparable. Arrows indicate short holds required for linear variable displacement transducer (lvdt) range offset in the slower tests. Note the decrease in $\Delta\mu_{direct}$ with slip at high velocity.

3.3. Friction Direct Effect

One of the most striking features of the friction data for tests carried out at either high velocity or high normal stress is the dramatic reduction in the size of the direct effect with increased slip (Figures 8 and 9). In order to quantify this effect for different test conditions we measure $\Delta\mu_{direct}$ at imposed upsteps for all the tests carried out.

Figure 8a shows $\Delta\mu_{direct}$ as a function of shear displacement for velocities in the range 0.001-10 mm/s at σ_n = 25 MPa. At the lowest velocities, $\Delta\mu_{direct}$ is essentially independent of displacement. In contrast, at higher velocity, $\Delta\mu_{direct}$ decreases dramatically with slip. The magnitude of the reduction with slip is systematically larger and occurs sooner (i.e., at lower displacement) with increased velocity. The inset to Figure 8a illustrates that $\Delta\mu_{evol}$ varies sympathetically in response to changes in $\Delta\mu_{direct}$. Changes in $\Delta\mu_{evol}$ therefore are not solely responsible for the transition in $(a-b)$ with increasing slip.

In Figure 8b we plot $\Delta\mu_{direct}$ for discrete ranges of shear displacement. At low velocity, data for all shear displacements plot together as expected from Figure 8a. However, at high ve-

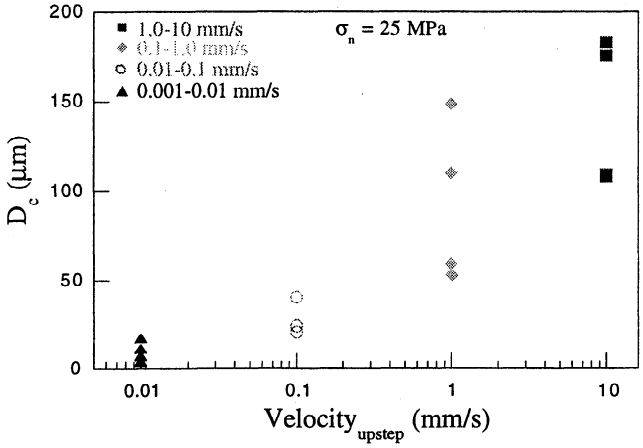

Figure 4. Critical slip displacement (D_c) as a function of upstep velocity for a range of experiments at σ_n = 25 MPa. D_c is systematically larger as a function of increasing velocity.

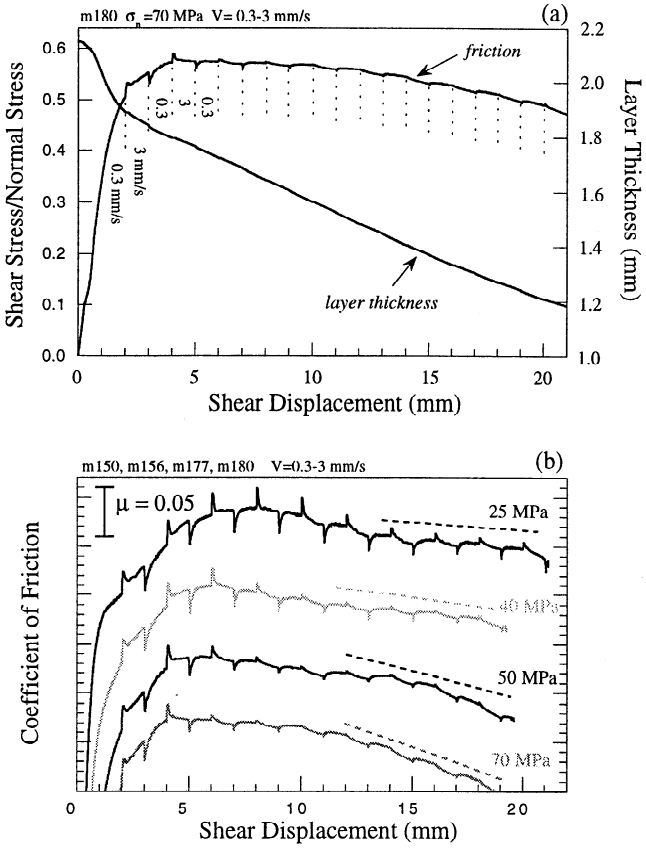

Figure 5. (a) Coefficient of friction and layer thickness as a function of shear displacement for a test carried out at normal stress of 70 MPa with velocity stepped between 0.3-3 mm/s. (b) Friction as a function of shear displacement for a range of normal stresses 25-70 MPa and velocity stepped between 0.3-3 mm/s. Curves are offset for clarity since friction values are comparable. Dashed lines indicate differences in the rate of weakening which increases with σ_n. The reduction in $\Delta\mu_{direct}$ with slip is greatest at high σ_n.

locity, $\Delta\mu_{direct}$ takes a range of values depending on slip. Velocity has a positive influence on $\Delta\mu_{direct}$ at small displacements (2-8 mm) and a negative influence at large displacements (14-20 mm). At intermediate shear displacement, $\Delta\mu_{direct}$ values are comparable for fast and slow tests.

We show the influence of normal stress on $\Delta\mu_{direct}$ in Figures 9a and 9b. All tests show a reduction in $\Delta\mu_{direct}$ with increasing shear displacement. The reduction occurs sooner and more precipitously for higher normal stresses. For small displacements, normal stress has negligible affect on $\Delta\mu_{direct}$, whereas at larger displacement, $\Delta\mu_{direct}$ decreases dramatically with normal stress (Figure 9b).

3.4. Dilatancy of Fault Gouge

In order to gain some insight into gouge layer evolution we study changes in layer thickness associated with step changes in velocity. To remain consistent with previous work [*Marone and Kilgore,* 1993], we calculate the parameter α as a measure of gouge layer dilatancy (Figure 10a). Here α is defined as $\alpha = \Delta h / \Delta \log V$ where Δh is the change in layer thickness (detrended for displacement dependent layer thinning) and V is load point velocity. In Figure 10b, α is plotted as a function of shear displacement. The lines connect points from an individual experiment, and common symbols indicate identical loading conditions. Experimental reproducibility is high, and data scatter is small compared to the effect of velocity. In all tests, α decreases with shear displacement. For a given displacement, α is systematically larger for higher-velocity. Furthermore, the reduction of α with slip is systematically larger for higher velocity tests. Data from *Marone and Kilgore* [1993] show comparable values to this study for corresponding conditions (Figure 10b).

We illustrate the influence of normal stress on α in Figure 10c. There is a decrease of α with displacement for all tests. The size of this overall decrease is similar regardless of normal stress; however, low normal stress tests show a gradual decrease with slip, whereas high normal stress tests show a more rapid initial decrease with little change in α during the latter half of the test.

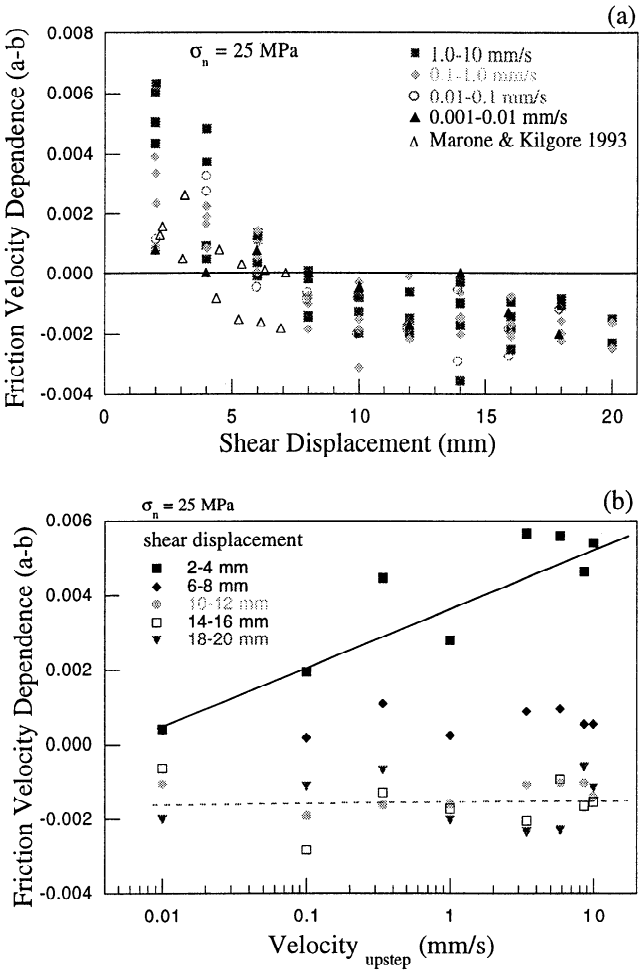

Figure 6. (a) Friction velocity dependence (*a-b*) as a function of shear displacement for velocities 0.001-10 mm/s and σ_n = 25 MPa. Several tests are plotted for each condition. Data from *Marone and Kilgore* [1993] for velocity 0.001-0.01 mm/s and σ_n = 25 MPa are superimposed. Note the transition from velocity strengthening to weakening with progressive slip. (b) Plot of (*a-b*) for the discrete displacement ranges shown as a function of upstep velocity. Lines indicate the trends at initial (2-4 mm, solid line) and final (18-20 mm, dashed line) displacements. Velocity has little influence on weakening for slip > 5 mm.

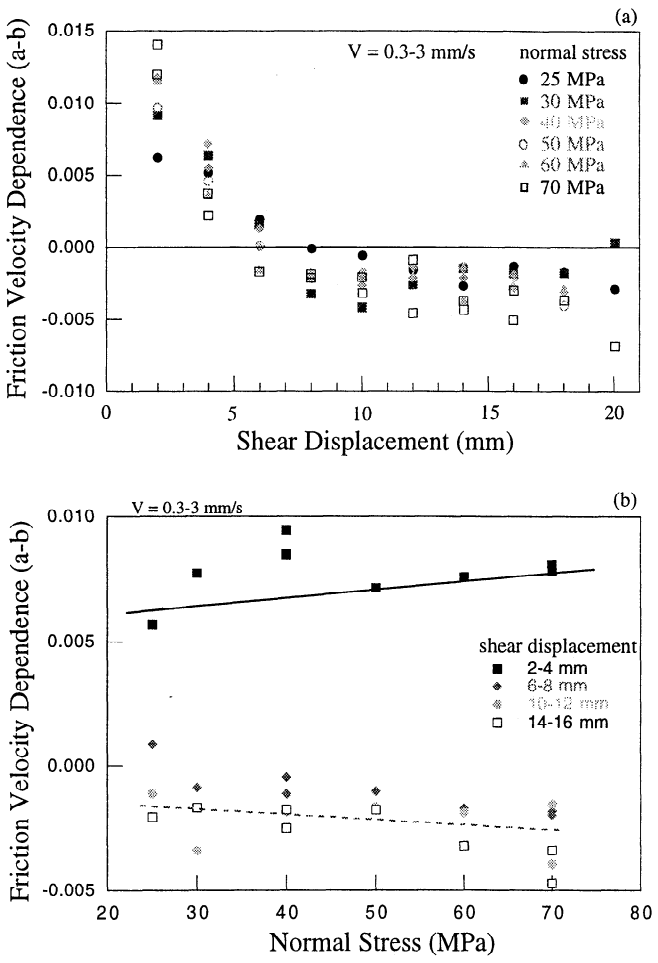

Figure 7. (a) Friction velocity dependence (a-b) as a function of shear displacement for normal stresses in the range 25-70 MPa. Repeated tests at 40 MPa and 70 MPa show reproducibility. All tests show a transition from velocity strengthening to weakening with slip. (b) Plot of (a-b) for discrete displacement ranges. Lines are visual aids indicating the trends of the data at small displacements (2-4 mm, solid line) and large displacements (14-16 mm, dashed line). The value of σ_n has a systematic but minor influence on (a-b).

3.5. Microstructural Observations

Microstructural observations were carried out on deformed gouge layers which had been impregnated with low-viscosity resin after unloading. Figure 11a is a backscatter scanning electron micrograph (SEM) image of a gouge layer subjected to 20 mm slip at a constant V = 0.5 mm/s while under σ_n = 50 MPa. This micrograph exhibits the general characteristics and fabric development observed for the range of conditions we consider here. By comparison with undeformed quartz gouge (Figure 11b), it is clear that significant comminution has occurred during slip. This grain size reduction is heterogeneous and indicates a distinct fabric. Relic pockets of less deformed material are indicated (A). Intensely comminuted zones lie along the gouge-forcing block interface (B), and in bands oriented at ~20° to the direction of shear (R). These granulated zones B and R are interpreted as regions of concentrated shear and correspond to the geometry of boundary and R_1 Riedel shears, respectively (Figure 11c) [*Logan et al.*, 1979]. Note that in Figure 11c we distinguish between layer-parallel shears located at the boundary (B) and within the layer (Y). Interestingly, we see no evidence for the development of through-going Y shears within the layer (Figure 11a). *Mair and Marone* [1999] indicate that deformation and localization of quartz gouge layers intensify with accumulated slip, but that for a given shear displacement, localization and comminution are comparable for gouge layers sheared at slow (10 μm/s) and fast (10 mm/s) velocities.

4. Discussion

4.1. Steady State Frictional Response and Microstructural Development

We observe a transition from a-b > 0 (velocity strengthening) to a-b < 0 (velocity weakening) as a function of shear displacement (Figures 6a and 7a). This result is consistent with previous work carried out at lower velocity for similar displacements [e.g., *Dieterich*, 1981; *Marone et al.*, 1992; *Beeler et al.*, 1996] and represents a change from intrinsically stable behavior to potentially unstable behavior. Notably, this transition is observed for all tests in this study (Figures 6a and 7a). With the exception of some initial strengthening observed at high velocity, under the conditions studied, V and σ_n have little systematic influence on friction velocity dependence. Hence for the conditions of our study (net slip < 30 mm, negligible shear heating, and slip rates < 10 mm/s), we do not observe the dramatic weakening that has been suggested as evidence for a self-propagating slip pulse mode of dynamic rupture [e.g., *Heaton*, 1990]. Our results are consistent with previous work by *Blanpied et al.* [1987, 1998], who also find no evidence for dramatic weakening at up to 3 mm/s. In fact, *Blanpied et al.* [1987, 1998] observe a systematic progression to velocity strengthening at high velocity which our data do not show. Recent work by *Goldsby and Tullis* [1998] shows that significant weakening can occur for larger displacements when shear heating may occur; however, the mechanism responsible has not been identified.

Marone et al. [1992] and *Beeler et al.* [1996] describe a strong correlation between friction velocity dependence and microstructural development, and note that for bulk distributed shear (a-b) is positive, whereas for localized shear along boundary-parallel "Y shears" (a-b) is more negative. The transition we observed in (a-b) as a function of increasing net slip may represent a corresponding transition from distributed to localized deformation, that is, the formation of shear bands within the gouge layer. Preliminary microstructural observations (Figure 11a) support this, indicating localization of shear (along R and B shears). Recent work [*Mair and Marone*, 1999] show that for slip of 5 mm, where (a-b) is positive, deformation is homogeneous and comparable in fabric to relic areas (region A, Figure 11a), suggesting distributed shear.

One important difference between our results and some previous work is that we observe no evidence for Y shears, despite reaching equivalent net slips [*Beeler et al.*, 1996; *Logan et al.*, 1992; *Blanpied et al.*, 1995]. This difference may be due to differences in layer thickness and net shear strains (layer thickness is ~2 mm in this study; ~ 1 mm in the work by *Beeler et al.* [1996]; ~0.58 mm in the work by *Blanpied et al.* [1995]). *Logan et al.*, 1992 showed that Y shears develop at a certain shear strain rather than shear displacement. Thus the thicker layers for our tests require larger shear displacement to

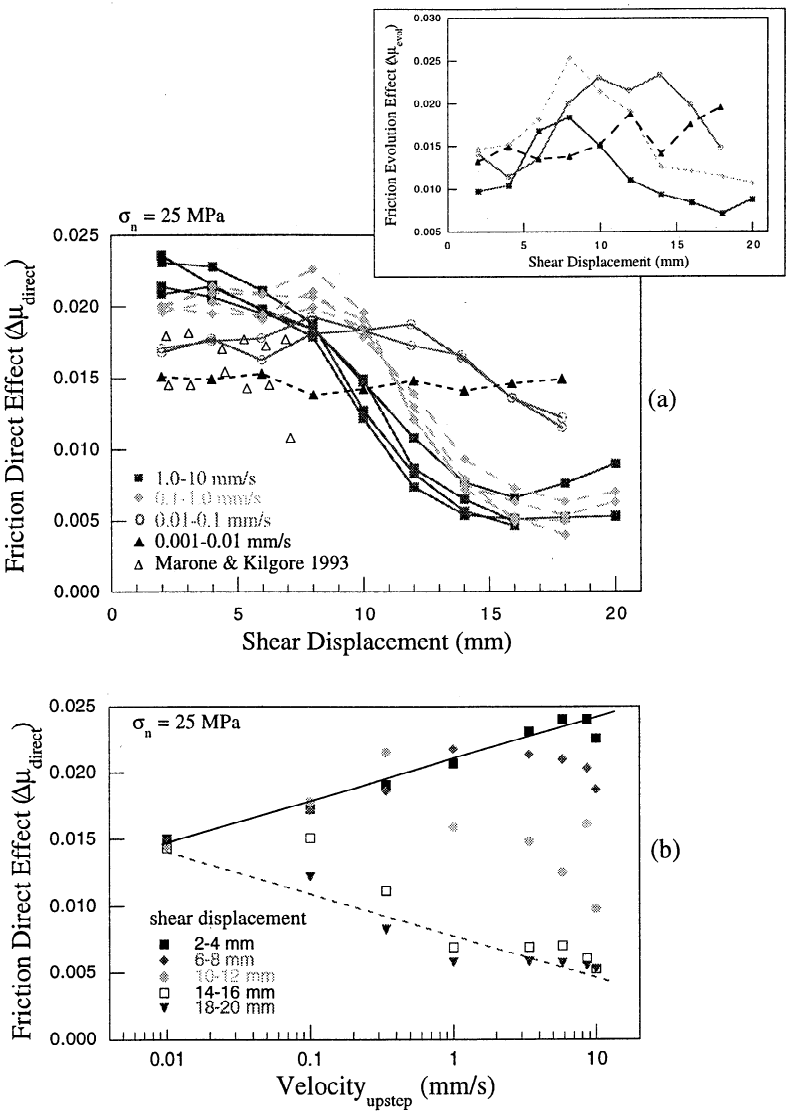

Figure 8. (a) Friction direct effect ($\Delta\mu_{direct}$) as a function of shear displacement for imposed velocity steps in the range 0.001-10 mm/s at σ_n = 25 MPa. Data from *Marone and Kilgore* [1993] for velocity 0.001-0.01 mm/s are superimposed. There is a systematic reduction in direct effect at high velocity with additional slip; however, at low velocity, $\Delta\mu_{direct}$ remains essentially constant throughout the test. Inset shows friction evolution effect $\Delta\mu_{evol}$ versus shear displacement. (b) $\Delta\mu_{direct}$ is plotted as a function of ustep velocity for discrete displacement ranges. Lines indicate the trends of the data at initial (solid line) and final (dashed line) displacements as in Figure 6b. A clear trend in the range of $\Delta\mu_{direct}$ values is observed with velocity.

reach the shear strains required to generate Y shears. We therefore propose that the transition to velocity weakening in our tests is associated with formation of the system of B and R shears.

Following from *Marone et al.* [1992] and *Beeler et al.* [1996], we argue that (*a-b*) is a proxy for degree of shear localization. Our friction and microstructural data [*Mair and Marone,* 1999] suggest that the degree of localization, and hence structural evolution, is similar regardless of loading rate. We note also that (*a-b*) is slightly sensitive to normal stress in the weakening regime (Figure 7b), which may affect fabric development.

4.2. Transient Response to Velocity Steps

Our data indicate that the friction direct effect is systematically influenced by both velocity and normal stress. In both cases, $\Delta\mu_{direct}$ reduces dramatically as a function of slip (Figures 8a and 9a). Studies of gouge sheared at low velocity [e.g., *Marone and Kilgore,* 1993] and on bare granite surfaces at high velocity comparable to this study [e.g., *Blanpied et al.,* 1987; *Kilgore et al.,* 1993; *Blanpied et al.,* 1998] indicate essentially constant $\Delta\mu_{direct}$ throughout the test. This suggests that we are observing a displacement dependent mechanism that operates only in gouge at high velocity. A systematically wider range of $\Delta\mu_{direct}$ values is observed with increasing velocity (Figure 8b). This indicates a more dramatic change in the size of the friction response with slip at high loading rates. This may imply that the influence of accumulated gouge damage on $\Delta\mu_{direct}$ is more important as a function of velocity.

Previous studies [e.g., *Lockner and Okubu,* 1983; *Lockner et al.,* 1986; *Chester,* 1988, 1994; *Blanpied et al.,* 1998] have investigated the influence of temperature on friction. In par-

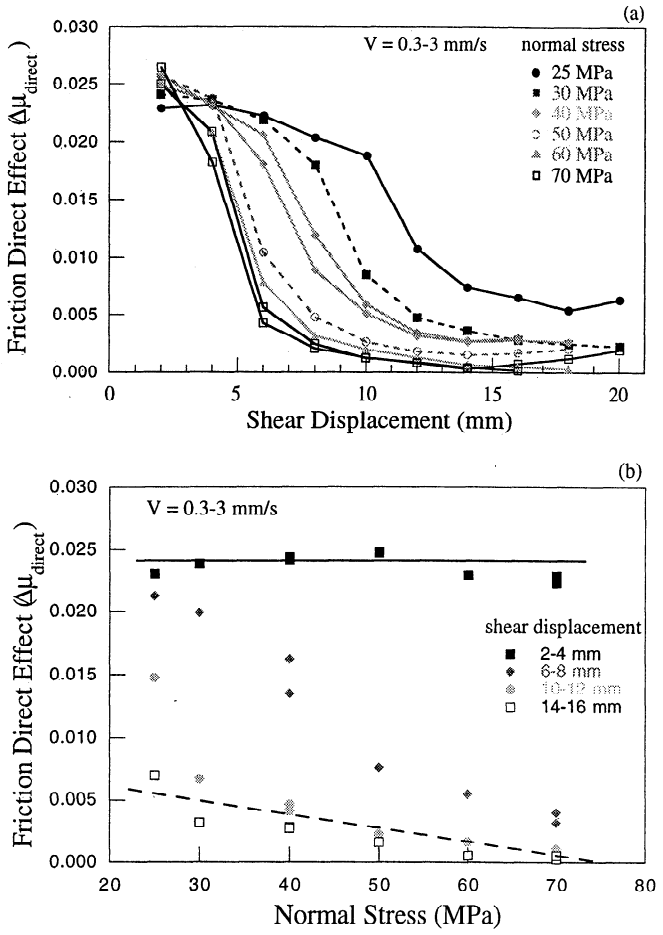

Figure 9. (a) Friction direct effect ($\Delta\mu_{direct}$) plotted as a function of shear displacement, for a range of normal stresses (σ_n = 25 - 70 MPa) and step changes in velocity between 0.3 and 3 mm/s. Note the effect of σ_n on $\Delta\mu_{direct}$. The decrease is rapid at high normal stress and more gradual at lower normal stress. (b) $\Delta\mu_{direct}$ for discrete displacement ranges plotted as a function of normal stress. Lines are aids indicating the main trends in the data for small (2-4 mm) and larger (14-16 mm) displacements. Normal stress has a minor influence on (a-b).

ticular, *Chester* [1994] showed that a sudden increase in temperature (~30°C) could reduce friction instantaneously. If this were associated with a step change in velocity, it could potentially reduce the size of the observed friction direct effect. We have measured temperature changes in our experiments near the gouge layers to determine whether shear heating could explain our friction observations [Mair and Marone, submitted manuscript, 1999]. However, temperature changes within the layer are < 8°C (for 20 mm slip, V = 10 mm/s, σ_n = 25 MPa), which is significantly lower than *Chester*'s [1994] measurements. Hence we argue that shear heating alone can not explain our observed changes in friction parameters with slip.

Blanpied et al. [1987] noted that the size of the friction evolution effect (b) was an important factor responsible for changes they observed in (a-b) as a function of velocity (Figure 6b). In our study we see that $\Delta\mu_{evol}$ changes in a complementary way to $\Delta\mu_{direct}$, resulting in little systematic change in the value of (a-b) with velocity.

The evolution distance (D_c), required to stabilize friction and reach a new steady state, increases as a function of velocity (Figure 4, Table 2). This potentially important result agrees with observations of bare gabbro at high velocity (up to 1 m/s) by *Tsutsumi and Shimamoto* [1997], but contrasts with the bare granite surface experiments of *Blanpied et al.* [1998], who observed no change in D_c with V over the range 10^{-2} to $10^{3.5}$ μm/s.

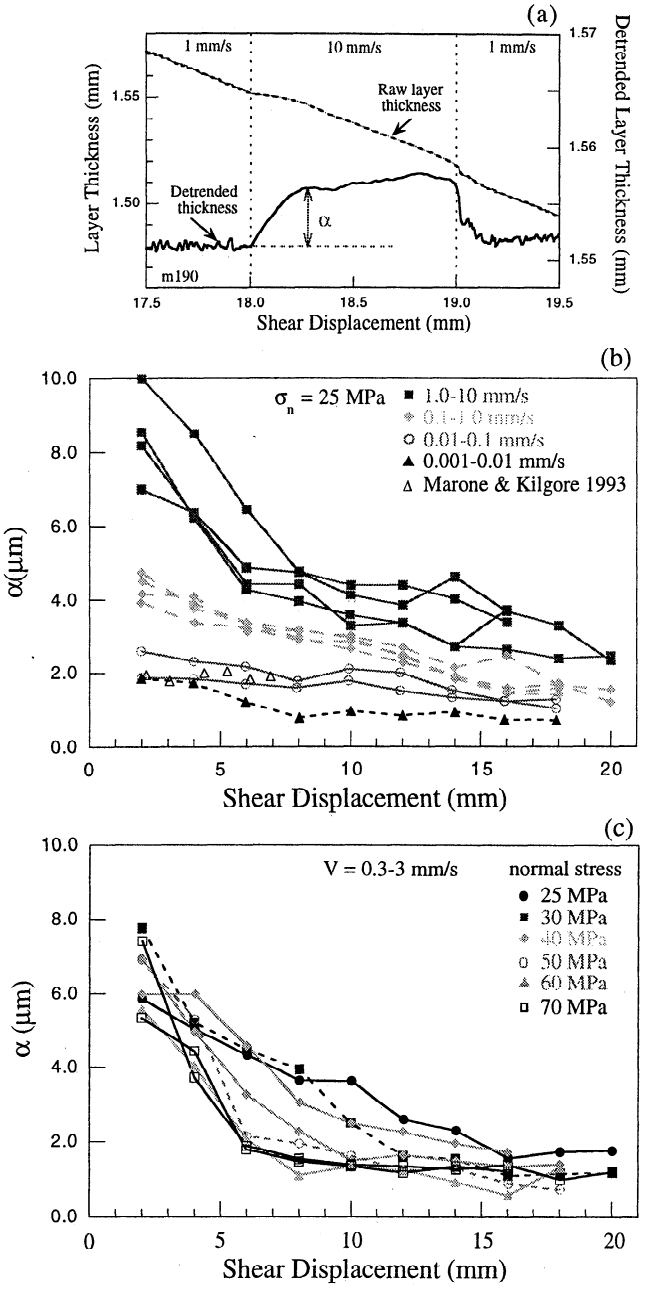

Figure 10. (a) Raw layer thickness data (dashed line) as a function of shear displacement showing dilation at an upstep and compaction at a downstep in velocity. Detrended layer thickness (solid line) is plotted, showing how α (arrow) associated with a velocity upstep is measured. (b) Plot of α as a function of shear displacement for a range of velocities (0.001-10 mm/s) and constant σ_n = 25 MPa. Note the experimental reproducibility in repeated tests. V has a systematic effect on the size of α and the reduction of α with slip. Data from *Marone and Kilgore* [1993] for velocity 0.001-0.01 mm/s are superimposed. (c) Plot of α as a function of slip for a range of σ_n (between 25 and 70 MPa) with velocity stepped between 0.3 and 3 mm/s. The systematic influence of σ_n is shown.

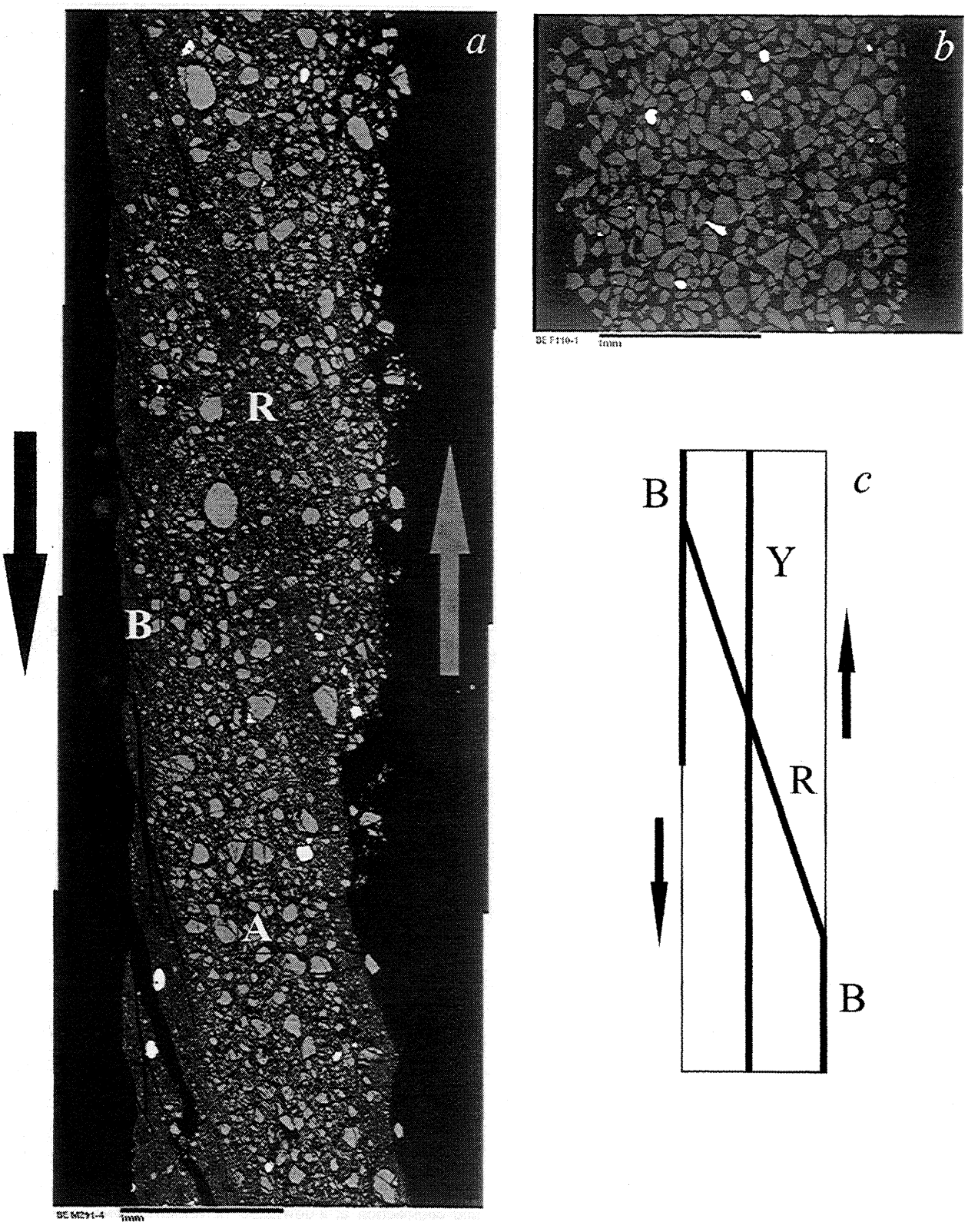

Figure 11. (a) Backscattered scanning electron micrograph (SEM) of a quartz gouge layer (initially 3 mm wide) deformed at $\sigma_n = 50$ MPa, $V = 0.5$ mm/s, shear displacement of 20 mm. The sense of shear is indicated by the arrows. Region A indicates relics of relatively undeformed material, B shows boundary shear, and R shows oblique (Riedel) shear. (b) SEM of an undeformed quartz gouge layer. (c) Schematic diagram showing some typical shear localization geometries in a gouge zone [following *Logan et al.*, 1979]. Following distributed shear and rapid comminution, evolution progresses from R (Riedel shears), to B (boundary shears), and subsequently to Y (boundary-parallel shears).

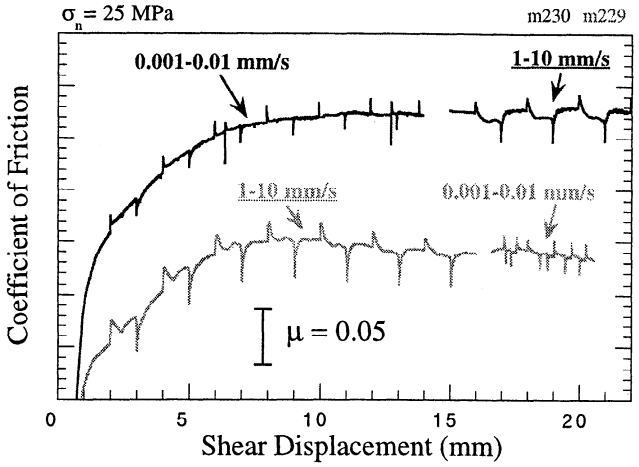

Figure 12. Friction plotted as a function of displacement for dual-velocity tests m230 and m229. The curves, m230 (dark curve) and m229 (light curve), are shifted for clarity since friction levels are comparable. In experiment m230, velocity was initially slow (1-10 μm/s) and then changed to fast (1-10 mm/s). In test m229 the opposite velocity transition was applied. Note the similar characteristics of segments of the tests carried out at equivalent velocities.

The gouge layer dilation (α) we observe at a step up in velocity, decreases with slip in all experiments (Figures 10b and 10c). This trend is consistent with previous experiments carried out on both gouge and bare surfaces [*Marone and Kilgore*, 1993; *Beeler et al.*, 1996]. We observe that α is a strong function of velocity, with high-velocity tests showing systematically larger dilation and more rapid decay of α with slip. High normal stress also promotes a more rapid decrease in α with slip; however, the initial and final values are similar for the range of normal stresses studied. Values of α for tests at V = 0.001-0.01 mm/s correlate well to previous work at comparable conditions [e.g., *Marone and Kilgore*, 1993]. However, dilation (α) of gouge layers during shear (this study) is notably larger than the dilation typically observed for bare surfaces [e.g., *Wang and Scholz*, 1994; *Beeler et al.*, 1996]. We can account for these differences by considering a shear band of finite thickness and by noting that shear within a gouge layer commonly involves the dilatant processes of particle rolling and grain fracture in addition to sliding, whereas shear along bare surfaces is primarily accommodated by sliding or asperity fracture.

Marone and Kilgore [1993] propose that α relates to the thickness of gouge participating in shear deformation. We argue that this interpretation is valid and use α to infer active shear band width. A decrease in α with slip, such as we observe, therefore suggests that the width of the active shear zone decreases with slip. Large α values and rapid decay in α with small displacement at high velocity imply that more gouge is initially participating in shear and that localization into shear bands with slip is more efficient than for lower velocities. The rapid decrease in α with slip observed at high σ_n (Figure 10c) implies that active gouge width decreases with slip more rapidly at high normal stress. Our observations imply that high velocity is associated with more dilatant deformation, while high normal stress inhibits dilatant processes [e.g., *Marone et al.*, 1990]. We observe no clear microstructural evidence for wider shear bands at high velocity [*Mair and Marone*, 1999]; hence we propose that the additional dilation observed at high loading rates is due to rolling or sliding of grains rather than fracture. These mechanisms will not induce significant grain comminution and hence may not be preserved as a permanent structure in the gouge.

Several of our observations suggest a memory of both net slip and velocity history. We see a progressive decrease in $\Delta\mu_{direct}$ with slip, which depends systematically on velocity. Loading rate also has a systematic influence on the variation of α with slip. As both $\Delta\mu_{direct}$ and α progressively change with slip, and are controlled by velocity, this suggests that some additional mechanism of gouge deformation may operate at high loading rates. It is already well established that friction parameters vary with net slip [*Dieterich*, 1981; *Beeler et al.* 1996; *Richardson and Marone*, 1999]; however, the role of velocity history in determining friction parameters is not well understood. In the next section we describe an investigation of this effect using novel dual-velocity experiments.

4.3. Influence of History on Friction Behavior

We have designed a set of dual-velocity experiments (see Table 1) to test the hypothesis that gouge evolution is a function of both velocity history and slip history. The majority of each test is run at one set of velocity steps, for example, slow (V=0.001-0.01 mm/s); then the end of the test is run at much faster rates (V=1-10 mm/s). Friction parameters are measured identically as for the standard velocity stepping tests. We investigate whether velocity history influences microstructural development in a way that is permanently recorded in the gouge. If so, the friction parameters at the end of a test will depend on previous velocity, in addition to net slip and current velocity. However, if velocity history is not recorded in the gouge, then friction parameters will depend on only net slip and V. We vary velocity history in dual-velocity tests and compare friction parameters to our standard tests.

Figures 12 and 13 show friction and dilation data as a function of slip for such tests. On the transition between fast and slow velocity (or vice versa) at around 15 mm, we lock the ram at a constant position to adjust loading rates, recording rates, and servo gain. There is a short data gap here, necessary to change data loggers. We assume that the influence of this short hold on subsequent friction is minor. The friction curves in Figure 12 are offset along the y axis for clarity, since the plots overlay one another. The initial stages of the tests are comparable to standard tests at equivalent velocities and shear displacements (cf. Figure 3b). After the velocity transition the curves for each experiment change to display features characteristic of the new velocity. The segments carried out at comparable V show clear similarities despite the different velocity histories. One of the main distinguishing features is the evolution distance D_c required to return to steady state after a velocity perturbation. D_c is intrinsically linked to current sliding velocity (Figure 4); however, qualitative observations from dual-velocity tests (Figure 12) reveal that this remains true irrespective of the velocity history.

In Figure 13a we show friction velocity dependence (a-b) as a function of slip for dual velocity tests, and the data are superimposed with standard (reference) velocity stepping tests (data from Figure 6a). The initial stages of the test yield (a-b) values that agree with standard tests at equivalent velocity and slip. A transition from fast to slow velocities results in a decrease of (a-b) toward more negative values, sug-

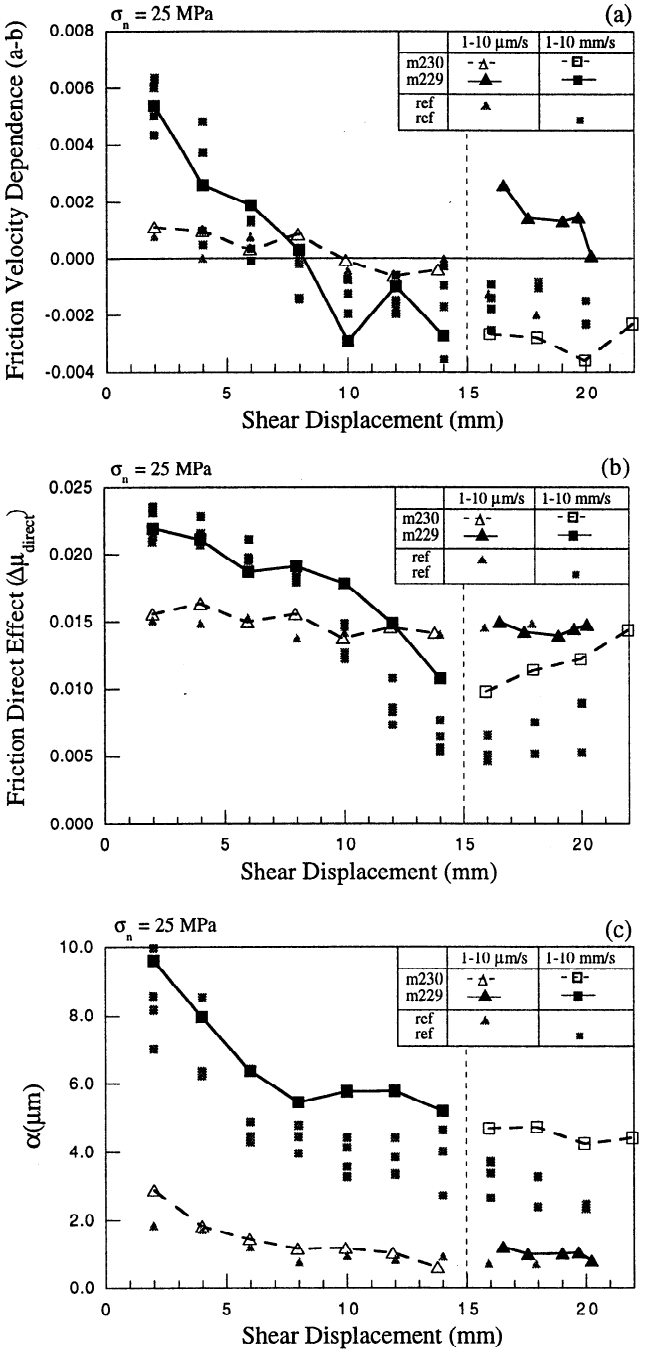

Figure 13. Friction and dilation data for dual-velocity tests. Open symbols (dashed curve) refer to experiment m230; solid symbols (solid curve) refer to test m229. In experiment m230, velocity was initially slow (1-10 μm/s) and then changed to fast (1-10 mm/s). In test m229 the opposite velocity transition was applied. Vertical dashed lines indicate the velocity transition at approximately 15 mm slip. Standard velocity stepping tests (ref) for comparable velocities are superimposed for reference as shaded triangles and squares. Triangles always signify velocity stepping between 1 and 10 μm/s, and squares always denote velocity stepping between 1 and 10 mm/s. (a) Plot of (*a-b*) as a function of slip for complementary dual-velocity tests, showing a jump in values upon a velocity transition. Note the opposite effect of an increase and decrease in V on (*a-b*). (b) $\Delta\mu_{direct}$ as a function of shear displacement. (c) Alpha (α) at each velocity upstep as a function of shear displacement. Note the systematic effect of the velocity transition on $\Delta\mu_{direct}$ and α.

gesting enhanced velocity weakening. Conversely, on a transition from slow to fast velocities, we observe an increase in (*a-b*) to a positive value, indicating velocity strengthening. Thus, (*a-b*) indicates a memory of past velocity state. This suggests that the simulated fault would be made seismically inactive (i.e., less prone to slip) due to sliding fast for a short period. Conversely, the fault has more seismic potential (i.e., the degree of instability is higher) after slipping slowly. These effects are reproducible in our experiments; however, their persistence at larger slip and for larger velocities is unknown.

Figure 13b shows the friction direct effect for dual-velocity tests and standard tests. Again, the initial stages of both dual-velocity tests are comparable to standard tests at corresponding values. At the transition to slow velocity, $\Delta\mu_{direct}$ jumps up to exactly the level of a standard slow velocity test. At a transition from slow to fast velocity, the size of $\Delta\mu_{direct}$ jumps down to a value that is comparable with that for a standard fast (1-10 mm/s) velocity test. These observations imply that $\Delta\mu_{direct}$ is independent of velocity history but is strongly influenced by net slip and the present velocity.

Figure 13c shows dilation of the fault gouge at a velocity upstep as a function of shear displacement. The initial part of the tests concurs with standard velocity tests for equivalent velocities and displacements. At a transition from fast to slow velocity, α jumps down to the level expected for equivalent slow (0.001-0.01 mm/s) tests. Conversely, at a slow to fast transition, α jumps up to values consistent with equivalent fast tests (1-10 mm/s) at corresponding shear displacement. These very clear jumps in α indicate that velocity history is not an important element for setting the physical factors that effect dilatancy (e.g., particle size distribution, shear band thickness, and spacing).

In summary, it is clear that the friction rate dependence (*a-b*) is significantly influenced by velocity history. Since this parameter is interpreted as a measure of fault stability, this result has potential importance in understanding slip history effects on real faults. For dual-velocity tests, transient friction parameters and dilation values return to the standard values at a switch in velocity. This suggests that although the current velocity conditions and the accumulated slip are important, the gouge retains little memory of past velocity perturbations.

4.4. Mechanisms of Deformation

Clearly, our experiments indicate some important correlations between friction parameters as a function of velocity, normal stress, and slip. We suggest that the transient frictional response ($\Delta\mu_{direct}$, $\Delta\mu_{evol}$, and D_c) and dilation are coupled. These parameters all vary systematically as a function of slip and are sensitive to changes in velocity and normal stress. A perplexing observation is that *a-b* evolves with slip and is influenced by velocity history but is insensitive to current V and only slightly affected by σ_n. In addition, we find some important differences between our results and those obtained at comparable velocities on bare granite surfaces.

Our experiments at high velocity show larger values of dilation and significant variations in both dilation and $\Delta\mu_{direct}$ with increasing slip. In contrast, bare surface experiments at comparable velocities [e.g., *Blanpied et al.*, 1998] show much smaller amounts of dilation and little or no change in $\Delta\mu_{direct}$ with slip. Hence the micromechanisms responsible for enhanced dilation in gouge may permit or encourage the varia-

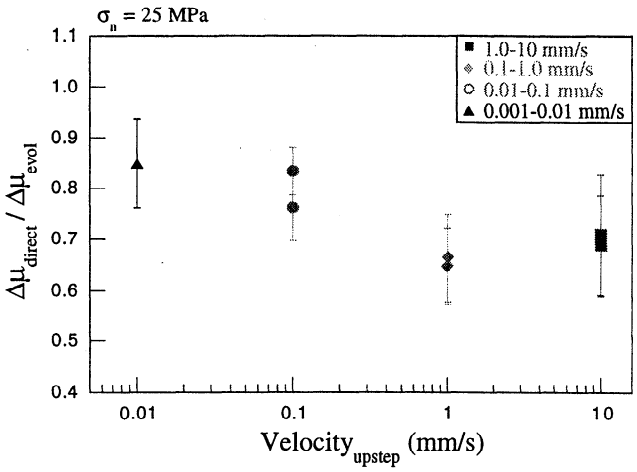

Figure 14. The ratio $\Delta\mu_{direct}$ / $\Delta\mu_{evol}$ (equivalent to a/b) shown for the velocity weakening regime, $(a-b)$ <0, as a function of upstep velocity. We plot mean values for each experiment. Error bars indicate plus and minus one standard deviation. The displacement trend is removed, and values are referenced to 15 mm slip. Data suggest a decreasing trend with increasing velocity.

tions we observe in the transient frictional response. Previous studies [e.g., *Marone et al.* 1990; *Sammis and Steacy,* 1994] have proposed a correlation between the transient frictional response and dilatancy based on a simple energy balance. *Marone et al.,* [1990] calculated the friction response due to dilatancy effects associated with a step change in velocity and obtained curves mirroring the main characteristics (if not the absolute values) of the observed friction curve. *Sammis and Steacy* [1994] suggested that the dilation at a velocity step produces a perturbation in friction that is proportional to the dilation rate. This perturbation then tends to zero when the gouge layer has dilated to a new steady state volume. This is consistent with our observations that transient and evolution effects are strongly correlated with dilation but that friction rate dependence is not.

It should be noted that *Beeler and Tullis* [1997] offer a contrasting view, suggesting that dilatancy is time, rather than slip dependent, and that time dependent dilatancy does not contribute to transient changes in friction. However, our data (Figure 2a) and frictional healing experiments on gouge [*Karner and Marone,* 1998; *Karner,* 1999] indicate that both slip and time dependent processes are important. Moreover, as pointed out by *Geminard et al.,* [1999], frictional strength scales with dilation, even if that dilation is time rather than slip dependent, and thus the *Beeler and Tullis* [1997] suggestion may not hold. The reasons for these differences are not well understood, and further work is needed.

A related issue is that of the connection between dilation and slip velocity. We observe systematically larger dilation at higher velocity. This may be because dilatant mechanisms (grain fracture and grain rolling) become more important at high velocity. *Marone et al.* [1990] suggested that low velocity favors grain boundary slip, since time dependent weakening processes (e.g., subcritical crack growth) have sufficient time to act. They argue that grain boundary slip alone cannot accommodate shear at high velocity, since time dependent processes cannot operate quickly enough, and that additional mechanisms (e.g., rotation and fracture) are required. Preliminary microstructural observations [*Mair and Marone,* 1999] suggest that the texture and deformation characteristics of our gouge layers are independent of velocity. Since this discounts the notion of enhanced grain fracture at high velocity, we tentatively attribute the observation of greater dilatancy for higher velocity to enhanced grain rolling.

4.5. Microstructural Interpretation

We expect that microstructures and permanent gouge deformation correlate, in some way, with the basic friction behavior and porosity and, moreover, that transient friction parameters may or may not be permanently preserved in the microstructure.

We have shown that friction evolves systematically with net slip and that constitutive parameters are essentially independent of sliding velocity but somewhat dependent on normal stress. We suggest that these observations reflect comminution and progressive granulation with slip, and enhanced comminution at higher normal stress. This view is consistent with preliminary microstructural observations [*Mair and Marone,* 1999]. We also see that $a-b$ is independent of sliding velocity, but is systematically affected by slip and σ_n. Since $(a-b)$ can be associated with degree of localization, these observations imply that gouge fabric development is progressive with accumulated slip and is affected by normal stress, but is insensitive to velocity. Our microstructural work [*Mair and Marone,* 1999] suggests the following progression: (1) homogeneous distributed deformation associated with $(a-b)>0$; (2) slip concentrated along Riedel shears associated with transitional behavior $(a-b)\sim 0$; and (3) development of boundary shears correlating to $(a-b) < 0$. With the possible exception of Y shear development, this evolution is consistent with previous studies [e.g., *Logan et al.,* 1992; *Marone and Scholz,* 1989; *Beeler et al.,* 1996].

Transient friction and dilation parameters indicate that more gouge is taking part in shearing during velocity perturbations at high V but there is no microstructural signal for this preserved in gouge layers. Also, $\Delta\mu_{direct}$ and α are independent of velocity history. The implication is that the dilatant deformation mechanism which becomes active at high V is not enhanced granulation but instead involves a nondestructive process such as grain rolling.

4.6. Implications for Earthquakes

We see no evidence for dramatic velocity weakening at high slip rates in the data presented thus far. However, theoretical studies show that the ratio a/b may be important in determining the mode of dynamic rupture [*Perrin et al.,* 1995; *Zheng,* 1997]. Figure 14 shows our data for this ratio (using the parameter $\Delta\mu_{direct}/\Delta\mu_{evol}$) as a function of V for the velocity weakening regime. The data suggest a decreasing trend with increasing V. If this trend were extrapolated to higher velocities typical of rupture, values $a/b \sim 0.2$ could be reached. According to *Perrin et al.* [1995] and *Zheng* [1997], this may suggest a condition in which slip pulse rupture is more likely. Also, an increase in D_c observed with increased slip could aid in the arrest of rupture by requiring additional slip before a lower stress condition is reached. Thus our laboratory evidence (a/b and D_c) is consistent with the notion that self-arresting slip pulse rupture is more likely at increased sliding velocities.

Although it is clearly speculative to directly compare our data to seismic faults, it may be possible to make some connection. We would expect natural faults to have undergone much more complex and varied behavior than our laboratory samples. However, by minimizing the level of complexity in sample and loading conditions, we can isolate variables that affect friction and gouge evolution. Our data show that granular fault gouge does not exhibit a strong change in frictional velocity behavior for velocities up to cm/s and thus if strong velocity weakening does occur in such materials it must initiate at higher velocities or at larger displacements. We note that *Goldsby and Tullis* [1998] apparently do find significant weakening for conditions similar to our tests, but for larger displacements and with significant shear heating; however the mechanism responsible has not been identified.

5. Conclusions

We report systematic, reproducible variations in laboratory friction of simulated fault gouge for a wide range of velocity and normal stress. Our main conclusions are as follows:

1. Data for low-velocity tests agree well with previous observations for corresponding conditions.

2. The friction rate dependence (a-b) undergoes a transition from positive to negative as a function of shear displacement with no major influence of velocity or normal stress. This indicates that strain localization is similar for high- and low-velocity tests, which is supported by microstructural observations. No dramatic velocity weakening is observed at high velocity or higher normal stress; however, relative weakening in the ratio a/b is enhanced at high V.

3. The friction direct effect is systematically influenced by velocity, causing it to decrease as a function of slip at high velocity and higher normal stress.

4. The dilation parameter α decreases as a function of slip. The value of α is initially larger and decreases more rapidly at high velocity, implying that more gouge is participating in shear. Similarly, the decrease in α is more rapid at higher normal stress, although the magnitude of the change is independent of normal stress. Microstructural studies suggest that the additional dilatant mechanism active at high V is grain rolling.

5. At high velocity, displacement dependent localization and microstructural development are coupled with an instantaneous friction response that depends on the current velocity state. The past velocity state does not influence the instantaneous friction; however, it significantly affects steady state friction.

Appendix

Figure A1 illustrates the resolution of our friction measurements for a sample rate of 3000/s at high velocities. We show the friction response to identical step changes in velocity (1-10 mm/s) at shear displacements of 10 mm (Figure A1a) and 20 mm (Figure A1b), representing the middle and latter stages of a typical test. We plot individual data points to highlight resolution. It is clear that we have adequate resolution to capture the direct and evolution effects throughout the entire test. We also see a reduction in the size of the direct effect associated with increasing slip.

Figure A2 highlights the reproducibility of the velocity stepping tests for identical test conditions. The absolute level of steady state friction is somewhat variable (0.5 to 0.65) and is difficult to reproduce from one experiment to another. However, the trend of friction as a function of displacement is comparable, and the reproducibility of the second-order friction effects is extremely good (see, e.g., Figure 10b). Data presented in the text were from tests that were repeated several times to check reproducibility.

Teflon plates were screwed to the sample side blocks to limit gouge loss from the unconfined edges of the sample. Preliminary tests (without plates) had displayed gouge loss which could affect microstructural evolution with accumulated slip. Examination of the gouge layers at the end of a test indicated that the addition of plates had successfully minimized this problem. The Teflon plates act to reduce overall geometric thinning (Figure A3). We also observe a small offset in friction levels, although the characteristics of the friction curve are comparable (Figure A3). We attribute the change in friction to layer thickness effects; however, note that the offset is of the same order as the scatter in reproducing friction levels (Figure A2). It is possible that the plates cause additional drag on the sample center block; however, this is

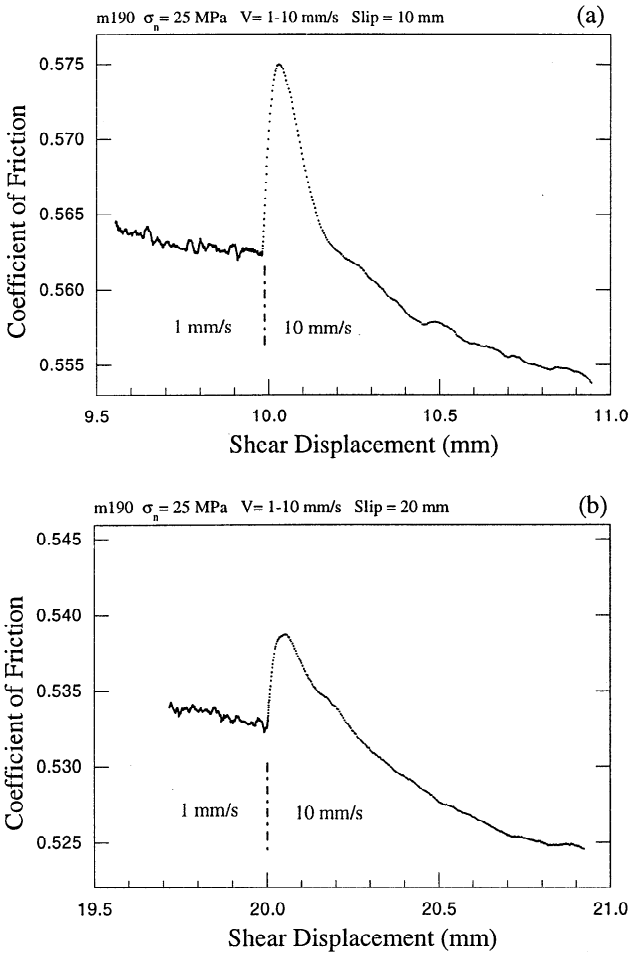

Figure A1. Resolution of friction measurements at high velocity: Friction (raw data) as a function of shear displacement for individual velocity steps (V = 1-10 mm/s) at (a) 10 mm slip and (b) 20 mm slip. The velocity step is indicated by the dashed line. Individual data points are shown to highlight resolution, which is clearly sufficient to capture the direct and evolution effects throughout the test.

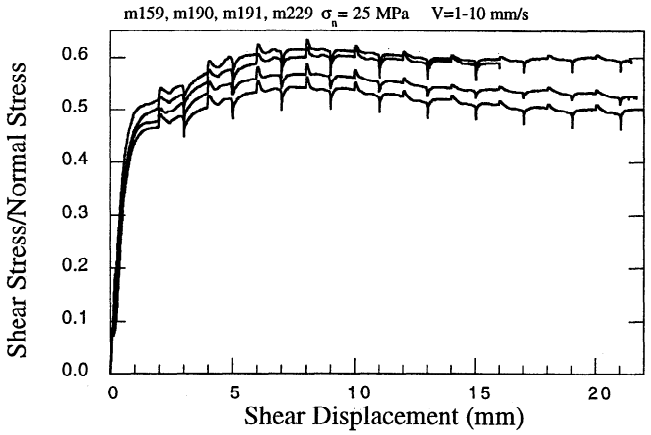

Figure A2. Reproducibility of tests: Friction as a function of shear displacement for four tests carried out at identical conditions (shown on the plot). Note the similarity between second-order effects despite the variability in base level friction.

very unlikely due to the extremely low coefficient of friction for Teflon sliding on steel.

We carried out extensive preliminary tests (>30 tests, not reported here) to refine the experimental technique and optimize the loading apparatus for attaining the high velocities (up to 10 mm/s) required in this study. With adjustments to the hydraulic pump flow rate and the control system, we can produce very clean, sharp velocity steps for loading rates up to 1 mm/s. Faster tests show a slight overshoot and then an undershoot in attaining a velocity of 10 mm/s. We quantified the sharpness of the change for velocity steps of 0.1-1 mm/s and 1-10 mm/s by taking the derivative of the shear displacement record with respect to time. An ideal response would be a boxcar function, but in practice it takes a finite time to attain the new velocity. The time taken to reach the upstep velocities is 0.02 s and 0.03 s in the fast (10 mm/s) and slower (1 mm/s) tests, respectively. The corresponding shear displacements are 100 μm and 20 μm, respectively. Results also indicate that the velocity overshoot is slightly larger at 10 mm/s; however, the size of the overshoot is essentially constant throughout a test with accumulated slip and between tests at the same conditions. This artifact cannot therefore account for any of the important systematic friction effects that we observe as a function of shear displacement. Also, these issues are only present in the fastest tests (10 mm/s), but the friction effects at 10 mm/s are a systematic extension of those for slower tests, indicating that the influence of this overshoot is negligible. Computer simulations were carried out to determine the size and influence of inertia at high loading rates [*Johnson*, 1997]. Results indicated that inertial effects are negligible for the range of velocities studied here, although effects may become significant at higher loading rates. Finally, despite the technical difficulties associated with making velocity steps at high velocity, it is possible to model the data using the actual load point velocity history, and this modeling indicates little effect of the loading history on friction [*Johnson*, 1997].

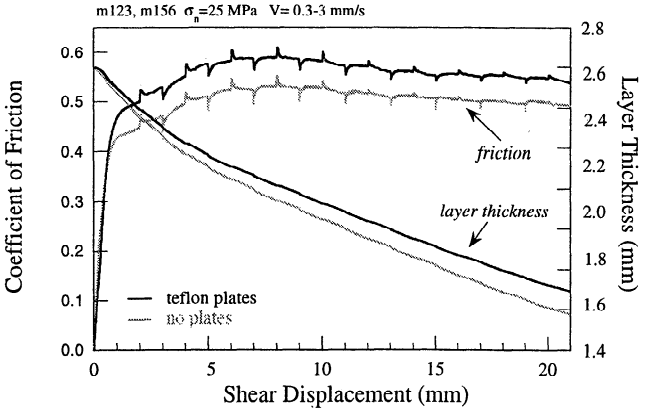

Figure A3. Influence of Teflon plates: Friction and layer thickness as a function of shear displacement for two tests at identical conditions (see plot). One sample had Teflon side plates attached; the other had no plates. Plates have a positive effect on both layer thickness and friction level.

Acknowledgments. We thank S. Karner, G. Hirth, J. Renner, U. Mok, Y. Bernabe, and M. Blanpied for stimulating discussions regarding this work. N. Chatterjee provided assistance with the SEM. We are grateful to J. Johnson, whose preliminary work on high-velocity tests provided a useful starting point for this study. We thank N. Beeler and an anonymous reviewer for thoughtful comments, which improved the paper.

References

Andrews, D.J., and Y. Ben-Zion, Wrinkle-like slip pulses on a fault between different materials, *J. Geophys. Res., 102,* 553-571, 1997.

Beeler, N.M., and T.E. Tullis, Self-healing slip pulses in dynamic rupture models due to velocity-dependent strength, *Bull. Seismol. Soc. Am., 86,* 1130-1148, 1996.

Beeler, N.M., and T.E. Tullis, The roles of time and displacement in velocity-dependent volumetric strain of fault zones, *J. Geophys. Res., 102,* 22,595-22,609, 1997.

Beeler, N.M., T.E. Tullis, M.L. Blanpied, and J.D. Weeks, Frictional behavior of large displacement faults, *J. Geophys. Res., 101,* 8697-8715, 1996.

Blanpied, M.L., T.E. Tullis, and J.D. Weeks, Frictional behavior of granite at low and high sliding velocity, *Geophys. Res. Lett., 14,* 554-557, 1987.

Blanpied, M.L., D.A. Lockner, and J.D. Byerlee, Frictional slip of granite at hydrothermal conditions, *J. Geophys. Res., 100,* 13,045-13,064, 1995.

Blanpied, M.L., T.E. Tullis, and J.D. Weeks, Effects of slip, slip rate, and shear heating on the friction of granite, *J. Geophys. Res., 103,* 489-511, 1998.

Chen, G., and C. Marone, Dynamic rupture growth and rupture barriers on faults with rate and state dependent friction (abstract), *Eos Trans. AGU, 76,* Fall Meet. Suppl., F408, 1995.

Chester, F.M., Temperature and rate dependence of friction for faults (abstract), *Eos Trans. AGU, 69,* 471, 1988.

Chester, F.M., Effects of temperature on friction: Constitutive equations and experiments with quartz gouge, *J. Geophys. Res., 99,* 7247-7261, 1994.

Dieterich, J.H., Time dependent friction and the mechanics of stick slip, *Pure Appl. Geophys., 116,* 790-806, 1978.

Dieterich, J.H., Modelling of rock friction, 1, Experimental results and constitutive equations, *J. Geophys. Res., 84,* 2161-2168, 1979.

Dieterich, J.H., Constitutive properties of faults with simulated gouge, in *Mechanical Behavior of Crustal Rocks,* edited by N.L. Carter, M. Friedman, J.M. Logan, and D.W. Stearns, *Geophys. Monogr. Ser.*, vol.24, pp.103-120, AGU, Washington, D.C., 1981.

Dieterich, J.H., and B.D. Kilgore, Direct observations of frictional contacts: New insights for state-dependent properties, *Pure Appl. Geophys., 143,* 283-302, 1994.

Geminard, J.-C., W. Losert, and J.P. Gollub, Frictional mechanics of wet granular material, *Phys. Rev. E, 59,* 5881-5890, 1999.

Goldsby, D.L., and T.E. Tullis, Experimental observations of frictional weakening during large and rapid slip (abstract), *Eos Trans. AGU, 79,* Fall Meet. Suppl., F610, 1998.

Heaton, T., Evidence for and implications of self healing slip pulses in earthquake rupture, *Phys. Earth Planet. Inter., 64,* 1-20, 1990.

Johnson, J., Laboratory study of rock friction at high velocity: Implications for constitutive laws, B.S. thesis, Mass. Inst. of Technol., Cambridge, 1997.

Karner, S.L., Laboratory analysis of restrengthening on simulated faults, Ph.D. thesis, Mass. Inst. of Technol., Cambridge, 1999.

Karner, S.L., and C. Marone, The effect of shear load on frictional healing in simulated fault gouge, *Geophys. Res. Lett., 25,* 4561-4564, 1998.

Kilgore, B.D., M.L. Blanpied, and J.H. Dieterich, Velocity dependent friction of granite over a wide range of conditions, *Geophys. Res. Lett., 20,* 903-906, 1993.

Lockner, D.A., and P.G. Okubu, Measurements of frictional heating in granite, *J. Geophys. Res., 88,* 4313-4320, 1983.

Lockner, D.A., R. Summers, and J.D. Byerlee, Effects of temperature and sliding rate on friction strength of granite, *Pure Appl. Geophys., 124,* 445-469, 1986.

Logan, J.M., M. Friedman, N.G. Higgs, C. Dengo, and T. Shimamoto, Experimental studies of simulated fault gouge and their application to studies of natural fault zones, in *Analysis of Actual Fault Zones in Bedrock,* edited by R.C. Speed and R.V. Sharp, *U.S. Geol. Surv. Open File Rep., 79-1239,* 305-343, 1979.

Logan, J.M., C.A. Dengo, N.G. Higgs, and Z.Z. Wong, Fabrics of experimental fault zones: Their development and relationship to mechanical behavior, in *Fault Mechanics and Transport Properties of Rocks,* edited by B. Evans, and T-F. Wong, pp.33-67, Academic, San Diego, Calif., 1992.

Mair, K., and C. Marone, Frictional and microstructural observations of fault gouge at high velocity (abstract), *Eos Trans. AGU, 80,* Spring Meet. Suppl., S329, 1999.

Marone, C., Laboratory-derived friction laws and their application to seismic faulting, *Annu. Rev. Earth Planet. Sci., 26,* 643-696, 1998.

Marone, C., and S.J.D. Cox, Scaling of rock friction constitutive parameters: The effects of surface roughness and cumulative offset on friction of gabbro, *Pure Appl. Geophys., 143,* 359-386, 1994.

Marone, C., and B. Kilgore, Scaling of the critical slip distance for seismic faulting with shear strain in fault zones, *Nature, 362,* 618-621, 1993.

Marone, C., and C.H. Scholz, Particle size distribution and microstructures within simulated fault gouge, *J. Struct. Geol., 11,* 799-814, 1989.

Marone, C., C.B. Raleigh, and C.H. Scholz, Frictional behavior and constitutive modelling of simulated fault gouge, *J. Geophys. Res., 95,* 7007-7025, 1990.

Marone, C., B.E. Hobbs, and A. Ord, Coulomb constitutive laws for friction: Contrasts in frictional behavior for distributed and localized shear, *Pure Appl. Geophys., 139,* 195-214, 1992.

Perrin, G., J.R. Rice, and G. Zheng, Self-healing slip pulse on a frictional surface, *J. Mech. Phys. Solids, 43,* 1461-1495, 1995.

Rice, J.R., and A. Ruina, Stability of steady frictional sliding, *J. Appl. Mech., 105,* 343-349, 1983.

Richardson, E., and C. Marone, Effects of normal force vibrations on frictional healing, *J. Geophys. Res.,* in press, 1999.

Ruina, A., Slip instability and state variable friction laws, *J. Geophys. Res., 88,* 10,359-10,370, 1983.

Sammis, C.G., and S.J. Steacy, The micromechanics of friction in a granular layer, *Pure Appl. Geophys., 142,* 777-794, 1994.

Scholz, C.H., Earthquakes and friction laws, *Nature, 391,* 37-42, 1998.

Scott, D.R., C. Marone, and C.G. Sammis, The apparent friction of granular fault gouge in sheared layers, *J. Geophys. Res., 99,* 7231-7246, 1994.

Tsutsumi, A., and T. Shimamoto, High-velocity frictional properties of gabbro, *Geophys. Res. Lett., 24,* 699-702, 1997.

Wang, W., and C.H. Scholz, Micromechanics of the velocity and normal stress dependence of rock friction, *Pure Appl. Geophys., 143,* 303-316, 1994.

Zheng, G., Dynamics of the earthquake source: An investigation of conditions under which velocity-weakening friction allows a self-healing versus crack-like mode of rupture, Ph.D. thesis, Harvard Univ., Cambridge, Mass., 1997.

Zheng, G., and J.R. Rice, Rupture propagation in classical enlarging crack mode versus short duration Heaton slip pulse mode (abstract), *Eos Trans. AGU, 75,* Fall Meet. Suppl., F441, 1994.

K. Mair and C. Marone, Department of Earth, Atmospheric and Planetary Sciences, Massachusetts Institute of Technology, 77 Massachusetts Avenue, Room 54-710, Cambridge, MA 02139. (e-mail: karen@barre.mit.edu; cjm@westerly.mit.edu)

(Received December 1, 1998; revised May 28, 1999;
accepted August 10, 1999.)